# Nanoscale Thin Films of Niobium Oxide on Platinum Surfaces: Creating a Platform for Optimizing Material Composition and Electrochemical Stability

Jennie I. Eastcott, Abhinav Parakh, Michael T. Y. Paul, Austin W.H. Lee, Matthew W. Bilton, Byron D. Gates*

*Department of Chemistry, Simon Fraser University, 8888 University Drive, Burnaby, BC V5A 1S6 (Canada). Telephone number (778) 782-8066, Fax number (778) 782-3765, Email address: bgates@sfu.ca

## Abstract

A nanoscale thin film of niobium oxide on a platinum substrate was evaluated for its influence on the electronic and chemical properties of the underlying platinum towards the oxygen reduction reaction with applications to proton exchange membrane fuel cells. The nanoscale thin film of niobium oxide was deposited using atomic layer deposition onto the platinum substrate. A film of niobium oxide is a chemically stable and electronically insulating material that can be used to prevent corrosion and electrochemical degradation when layers are several nanometers thick. These layers can be insulating if sufficiently thick, and may not be sufficient to protect the platinum from corrosion if too thin. An ~3-nm thin film of niobium oxide was fabricated on the platinum surface to determine its influence on the electronic and chemical properties at the interface of these materials. The atomic layer deposition process enabled a precise control over the material composition, structure, and layer thickness. The niobium oxide film was evaluated using cyclic voltammetry and electrochemical impedance spectroscopy to evaluate whether a balance could be found between the inhibition of platinum degradation and electronic insulation of the platinum for use in proton exchange membrane fuel cells. The 3-nm thin niobium oxide film was found to be sufficiently thin to permit electronic conductivity while reducing the incidence of platinum dissolution.


**Keywords:** proton exchange membrane fuel cell, atomic layer deposition, niobium oxide, platinum, degradation

## Introduction

To ensure competitiveness in the growing alternative energy sector for automotive applications, the next generation of proton exchange membrane fuel cells (PEMFCs) must exhibit enhanced durability under a variety of operating conditions. The U.S. Department of Energy (U.S. DOE) year 2020 durability targets specify that membrane electrode assemblies (MEAs) designed for automotive applications must be able to survive 5000 hours with cycling, as well as a start-up/shut down durability of 5000 cycles.[1] Typical PEMFC electrode layers consist of a carbon-supported platinum catalyst mixed with a proton-conducting polymer (ionomer). To achieve high durability in harsh fuel cell operating conditions, new catalyst, support, and ionomer materials must be investigated and an improved understanding of novel catalyst-support interactions is necessary. Improved durability must come with an overall cost reduction.[1] The various strategies for mitigating the durability shortcomings required for U.S. DOE compliant fuel cell operation each have their own benefits and challenges. For the cathode catalyst layers, aspects of the catalyst layer structure, such as ionomer type, ionomer loading, porosity, and layer thickness must be optimized to maintain conversion efficiency after modifying the catalyst/support properties.[2]

The carbon support used for many commercial platinum catalysts is thermodynamically inclined towards corrosion throughout the entire fuel cell operation voltage range.[3] During start-up and shut down of the fuel cell, potentials up to 1.5 V are produced and the carbon support degradation is accelerated[3], leading to loss of platinum surface area and decreases to both hydrogen oxidation reaction (HOR) and oxygen reduction reaction (ORR) reaction efficiencies. Robust alternatives to carbon supports have been investigated to preserve prolonged functionality of the platinum catalyst. In recent years, metal oxides such as $TiO_x$, $WO_x$, $SiO_x$, $NbO_x$, and $TaO_x$ ($x \leq 2$) have been of interest as both catalysts and catalyst supports due to their multitude of fabrication options (e.g., sol gel, ALD/CVD, magnetron sputtering, mechanical mixing), variety of oxide states, and their robust nature for fuel cell

environments.[3–7] One of the difficulties with metal oxide use in a fuel cell environment is that changes in structure and, in some cases, dissolution can occur during electrochemical cycling in acidic environments.[3] Exposure to different oxidative or reductive environments can change the nature of the metal oxide species and impact characteristics such as catalytic function and durability. Niobium oxides can exist as electronically conductive ($NbO_2$), insulating ($Nb_2O_5$), and semi-conducting forms ($NbO_X$), and can change between these structures with electrochemical cycling in different pH environments.[8] As platinum is the typical ORR catalyst for fuel cell applications, it is imperative to characterize these changes, as well as the influence of the presence of platinum catalyst, on supports such as niobium oxides under the types of fuel cell voltage conditions experienced during operation through catalytic cycling. Exploring changes in the surface characteristics of niobium oxides in the presence of platinum during voltage cycling will lead to a better understanding of the role that niobium oxides can play and can lead to an optimization of their use as support materials for fuel cell catalyst layers.

Niobium oxide has been investigated for applications such as solar cells[9,10], batteries[9], semiconductors/electronics[9,11], catalysis[9,12], optics[13–15], and as a coating for automotive[13] and biomedical devices for use *in vivo*.[9,16,17] The robust chemical stability, dynamic optical properties, high refractive index, and array of amorphous and crystalline phases for $Nb_2O_5$ make it a very popular material to study.[13] Niobium oxides are known to have strong metal-support interaction (SMSI)[18–20] properties and are, therefore, appealing candidates as platinum catalyst supports. Niobium oxides also have a high corrosion resistance and are thermodynamically stable.[16,21]

Nanoparticles of $Nb_2O_5$ have a low electrical conductivity.[22] The $Nb_2O_5$ can, however, have different degrees of hydrophilicity depending on whether it is amorphous or one of 12 crystalline morphologies[9], and this if coupled with a high affinity to platinum would help decrease the need for a high surface area support.[3] Additionally, stable oxide films could be employed as coatings for fuel cell

86 catalysts to prevent mechanisms of platinum degradation. These oxide films would be required to be
87 both porous and sufficiently thin so as to not disrupt electronic conductivity and gas permeability.

88 To date, there is limited research related to niobium oxides and their applicability to fuel cells.
89 Rocha *et al*.[19] determined that the addition of even small amounts of $Nb_2O_5$ to Pt catalysts for PEMFCs
90 enhanced CO tolerance (up to 100 ppm CO in the hydrogen feed) due to very high SMSIs. Huang *et al*.[23]
91 found that mixed Nb-Ti oxides can exhibit high electrical conductivity and electrochemical stability,
92 lending itself to be a potentially suitable Pt support as it had a positive impact on ORR activity and fuel
93 cell performance after accelerated durability cycling. Similar results were obtained by Chhina *et al*.[24]
94 regarding mixed Nb-Ti oxide supports. Zhang *et al*.[22] investigated growth of niobium oxide (as
95 $NbO_2$)/carbon nanotube (CNT) supports for platinum fuel cell catalysts. No considerable loss of
96 electrochemical surface area was evident after 10 000 complete electrochemical cycles within the
97 region of 0.6 to 1.1 V versus RHE. Though some losses in electrochemical surface area and ORR activity
98 were observed when cycling over a wider voltage range (0.5 to 1.4 V versus RHE), the degradation was
99 less than for similar Pt/CNT electrodes lacking the $NbO_2$ layer. Sasaki *et al*.[20] deposited very small
100 quantities of platinum on carbon-supported $NbO_2$ or $Nb_2O_5$ particles, determining that while the
101 $Pt/NbO_2/C$ particles had a high mass activity and durability, the $Pt/Nb_2O_5/C$ was able to achieve similar
102 mass activities to traditional Pt/C electrocatalysts.

103 The method of niobium oxide preparation can heavily influence the properties of the final
104 product. Material stresses, crystallite grain size, purity, thicknesses, and crystalline state are imparted by
105 the methods chosen for preparing films of niobium oxide.[9] Films of $Nb_2O_5$ can be produced using a
106 variety of techniques, which include: (i) sol gel[9,18,20,25,26]; (ii) magnetron sputtering[4,13]; and (iii) atomic
107 layer deposition.[11,27,28] Benefits of employing atomic layer deposition (ALD) include the precise control
108 of material composition, structure, and layer thickness. The ALD process is a form of chemical vapour
109 deposition that differs from traditional forms due to its ability to alternatively expose the desired

substrate to more precise amounts of precursors through pulsing and cycling of volatile reagents.[11] To create a metal oxide layer, at least two precursors (e.g., a volatile metal species, and either oxygen or ozone or water) are sequentially introduced into a reaction chamber that contained the substrate of interest under partial vacuum. Each reactant is introduced for a specific period of time and the chamber purged before introducing the subsequent reactant(s). This process is repeated for a series of cycles to promote film growth on a timescale of fractions of an angstrom per cycle. This thin film growth technique enables a precise control over the resulting thickness and composition. Atomic layer deposition has been used for the fabrication of semiconductors and nanomaterials for numerous applications since the layers produced can be conformal to the underlying substrate and are free of pinhole defects.[11]

In this study, nanometer-thin films of $Nb_2O_5$ were constructed onto platinum supports using ALD techniques with the goal of determining whether such thin niobium films can preserve platinum activity during electrochemical cycling without greatly impeding electronic conductivity. Improved understanding of this interface will drive development of materials with enhanced performance and robustness while balancing material cost. The use of ALD facilitated growth of thin films on the order of less than one angstrom per cycle in a well-controlled environment. To the best of our knowledge, nanometer-thin films of niobia produced via ALD have not been used to resist catalyst or catalyst support degradation for fuel cell environments. To fully characterize the interface between platinum and niobia, we examined changes in surface properties of the two materials to understand the limits of their conductive capabilities and electrochemical stability as suited to PEMFC applications.

## Experimental

### Fabrication of platinum substrate layer by physical vapor deposition

Silicon wafers were used as substrates for the platinum electrodes, which were prepared by physical vapor deposition (PVD) techniques. Silicon wafers used in these studies were four-inch, p-type, test-grade, single-side-polished (100) silicon wafer with a resistivity of between 1 and 10 Ω·cm. These substrates were purchased from 4D LABS at Simon Fraser University (SFU). The silicon wafers were thoroughly cleaned in a Class 100 clean room with a sequence of acetone, isopropyl alcohol, and oxygen plasma (Technics, PEII-A) at 280 mTorr and 300 W of plasma prior to PVD treatment. This cleaning process was performed to remove organic residue from the surfaces of the polished silicon wafer for improved adhesion of the deposited films during subsequent processing steps. Metal deposition was performed using a physical vapor deposition system (Kurt J. Lesker PVD75) with the chamber pressure <2.00E-6 Torr. An ~5-nm thick chromium layer was deposited with thermal evaporation technique to ensure sufficient adhesion between the silicon wafer and the platinum layer. The platinum layer was deposited using electron beam assisted evaporation technique with a target thickness of ~200 nm. The thickness of thin films during the deposition was monitored using a quartz microbalance (Sigma SQM-242) installed within the PVD system.

**Fabrication of $Nb_2O_5$ thin films by atomic layer deposition**

A nanoscale thin films of $Nb_2O_5$ was prepared via a thermally assisted ALD process using a Cambridge NanoTech Fiji F200 in 4D LABS at SFU. Briefly, the set-up includes a sample chamber with a load lock that moves substrates into the reaction chamber. The reaction chamber was placed under vacuum and purged with high purity argon gas (99.999%, Praxair). The Pt coated on the polished silicon substrates (~2 cm x 2 cm) were loaded into the ALD chamber for a sequential reaction with tert(butylimino)tris(diethylamido)niobium (Sigma Aldrich), or TBTDEN, and $H_2O$ as precursors. The chamber and substrate temperatures were set to 250 $^{o}$C and 65 $^{o}$C, respectively, and the pressure was held at 0.0156 Torr in the main chamber. The TBTDEN and $H_2O$ precursors were each heated to 65 $^{o}$C

overnight prior to the deposition process. The argon carrier gas and argon plasma flow rates were set to 60 sccm and 200 sccm, respectively. The TBTDEN was introduced into the chamber for 1 s, followed by the introduction of argon gas for 0.5 s. After 3 of these cycles, the $H_2O$ was introduced to the chamber for 0.06 s followed by a 0.5 s argon gas purge. This process was repeated for a total of 270 times to achieve the desired target thickness of 3 nanometers. After deposition, the samples were cooled to room temperature under an argon atmosphere. The growth rate for the $Nb_2O_5$ film was determined *vide infra* to be 0.1 Å/cycle under these reaction conditions. A schematic of the process can be found in Fig. 1.

## Physical characterization

### Focused ion beam/scanning electron microscopy

To evaluate the thickness of the ALD films, a focused ion beam (FIB) lift-out procedure was performed on the sample targeted to contain a 3-nm thick $Nb_2O_5$ film. The FIB process used an FEI Helios Dual-Beam scanning electron microscope (FIB-SEM) located in 4D LABS at SFU. An ~16-nm thick layer of carbon and a ~20-nm thick layer of iridium were coated onto the sample using a Leica EM ACE600 high-vacuum sputter coater (4D LABS). For subsequent STEM-EDS analysis, these layers allowed for adequate separation between the platinum substrate and the protective layer of platinum subsequently deposited using the gas injection system (GIS) within the FIB-SEM as necessary to assist with the sample lift-out procedure. An ~10-µm wide by 3-µm deep cross-section, and a sample thickness of ~2 µm, was milled in the FIB-SEM using a gallium ion-source. The sample was then attached to an Omniprobe copper lift-out grid, and further thinned by to ~30 nm by milling with the gallium ion-source.

The composition of the 3 nm $Nb_2O_5$ film was determined using energy dispersive X-ray spectroscopy (EDS), acquired using a FEI Osiris S/TEM equipped with a Super-X EDS detector system located in 4D LABS at SFU. Measurements were taken at 450 000x magnification at 200 kV.

**Electrochemical characterization**

Sufficiently thin layers of $Nb_2O_5$ may offer protection to platinum surfaces to make them less susceptible to platinum dissolution and Ostwald ripening. The $Nb_2O_5$ is, however, electrically insulating and will impede the flow of electrons and reactants to reaction sites if the film is too thick. Electrochemical potential cycling was used to evaluate the functionality of the $Nb_2O_5$ coating in an environment representative of a fuel cell.

Electrochemical measurements were performed with a Biologics Potentiostat (Model SP-150) using a three-electrode set-up in 0.09 M $H_2SO_4$ (Fisher Scientific, ACS Grade) while holding the electrolyte at room temperature. The three electrodes included a carbon counter electrode, Ag/AgCl reference electrode (CH Instruments, part no. CHI111), and the $Nb_2O_5$/Pt sample as the working electrode. Note that since the ALD process produces a conformal layer, all edges of the PVD substrate were coated with the $Nb_2O_5$ coating. A flat copper clip soldered to a copper wire was used to attach a portion of the working electrode devoid of $Nb_2O_5$ layer to the electrochemical circuit. A portion of the working electrode with an area of ~1 cm x ~2 cm was submerged in the electrolyte. After analysis, the submerged portion of the surface had changed colour and its exact area was measured for surface area normalization of the results. A platinum film prepared without the $Nb_2O_5$ coating was used for comparison. The electrochemical set-up is shown in Fig. 2.

Prior to electrochemical analysis, the system was purged with nitrogen gas (Praxair, 99.998%) to displace dissolved oxygen. The cell was sealed to reduce the introduction of oxygen gas during the experiment. To sufficiently evaluate the ability of $Nb_2O_5$ to protect the platinum surfaces from degradation, an accelerated stress test (AST) protocol was used to encompass a range of potential degradation mechanisms. All voltage reported are versus the reversible hydrogen electrode (RHE). To evaluate the ability of the $Nb_2O_5$ to prevent degradation in a wide range of fuel cell voltage conditions, a

wider potential cycling range was used similar to those proposed by Pizzutilo *et al.*[29] The samples were subjected to cyclic voltammetry (CV) experiments, scanning in the region of 0 V to 1.25 V (versus RHE) at 100 mV/s for 100 complete scans to condition the surfaces, followed by 10 complete scans in the same potential range at 50 mV/s to determine the electrochemically active surface area (ECSA) at the beginning of test (BOT). An average ECSA was calculated using the $8^{th}$, $9^{th}$, and $10^{th}$ scans. Linear sweep voltammetry (LSV) was performed at 5 mV/s and the current was recorded every 1 mV from 1.1 V to 0.2 V (versus RHE). Three LSV scans were obtained after the initial CV scans, and LSV plots consist of the average of these three scans. Electrochemical impedance spectroscopy (EIS) measurements were collected at a DC bias potential of 0.4 V (versus RHE) across a frequency range from 100 kHz to 0.1 Hz. The finite transmission-line model developed by Pickup *et al*. was used to analyze the EIS data.[30] The AST involved cycling the sample from 0 V to 1.3 V (versus RHE) at 200 mV/s for a total of 5 000 cycles. After every 1 000 cycles, the ECSA, LSV, and EIS test protocols were implemented to monitor degradation.

## Results and Discussion

### Fabrication of platinum thin film

The successful fabrication of the platinum thin film layer was confirmed using scanning profilometry. The profile, shown in Fig. 3, suggests that the total thickness of the platinum layer is between 205 to 210 nm. The PVD process required ca. 5 nm of chromium as an adhesion layer for the subsequent deposition of the ca. 200-nm thick platinum. This result suggests that the targeted metal thickness was achieved by the PVD process.

### Fabrication of nanometer scale thin films of $Nb_2O_5$

Atomic layer deposition can very finely control the deposition of a range of materials. It is capable of achieving a uniform layer thickness down to a few angstroms. There is an inherent difficultly to evaluate the thickness of the films prepared at this scale. Many techniques can have difficulty to resolve the properties of a nanometer-thin layer from the properties of the substrate. Traditional methods of verifying layer thickness, such as scanning electron microscopy and ellipsometry, were either unable to recognize the existence of the layer or require advanced models to determine the precise thickness. Our attempts to characterize the $Nb_2O_5$ layers with interferometry, ellipsometry, and high-resolution transmission electron microscopy (TEM) were unsuccessful. The layers proved to be too thin in contrast to the properties of the platinum substrate to accurately resolve the $Nb_2O_5$ by any of these methods.

The EDS spectrum from a section of the substrate covered with the niobium oxide layer is shown in Fig. 4. The niobium oxide layer is sufficiently thin that a strong contribution from the platinum layer is evident. Layers of carbon, iridium, and platinum were successively deposited onto the sample and a thin cross-section lifted out using FIB techniques to help resolve the nanometer-thin film of $Nb_2O_5$. Fig. 5a to 5d display individual elemental EDS maps acquired for the 3-nm $Nb_2O_5$ nanometer-thin film after sampling by FIB assisted lift-out. Platinum (Fig. 5a) is visible as both the PVD substrate and as part of the FIB sample preparation. Niobium appears visible in many regions (Fig. 5b), possibly due to the overlap of the first Nb peak with the Pt peak (Fig. 4). The brightest region in Fig. 5b is the actual $Nb_2O_5$ film. Oxygen (Fig. 5c) appears in all regions, but a concentrated oxygen region in seen in Fig. 5c in the same region as niobium is detected in Fig. 5b, indicating the successful deposition of niobium oxide species. The iridium band in Fig. 5d is a product of the FIB sample preparation.

The combined elemental map is seen in Fig. 6 (a and b). A layer of $Nb_2O_5$ is visualized (red region) between the PVD deposited platinum (green region) and FIB deposited carbon (black region) layers. The thickness of the $Nb_2O_5$ layer was estimated to be ~3-nm from these results, which was the target thickness for the sample.

## Electrochemical characterization

Results of electrochemical cycling are summarized in Table 1. As the samples were created via PVD and did not contain platinum nanoparticles, a geometric surface area of the electrolyte-immersed electrode surface was used for normalization of ECSA values. Exposure of each sample to the electrolyte and, thus, the area to undergo electrochemical cycling was approximately 2 cm x 1 cm (measurements to 0.01 cm used for area calculation), plus the 200 nm thick edges. It is expected that no region of bare platinum is exposed to the electrolyte for the $Nb_2O_5$-coated sample as the ALD process is conformal. The beginning of test (BOT) cyclic voltammetry scans are shown in Fig. 7. The 3-nm $Nb_2O_5$ film does not appear to considerably inhibit the electronic conductivity of the Pt layer. While the ECSA decreased for both samples, the niobium oxide coated sample exhibited a higher retention of ECSA (26.5 ± 1.7% loss) compared to the bare platinum film (33.7 ± 5.0 % loss). Fig. 8 depicts LSV scans taken at BOT and EOT for each sample. Both the bare Pt and $Nb_2O_5$-coated samples have almost identical LSV profiles between 0.75 to 1.1 V vs RHE and almost the same value at -0.03 mA/cm$^2$ (0.793 V and 0.784 V, respectively). After the AST protocol, at -0.03 mA/cm$^2$ there is a 71 mV shift in the onset potential for the bare Pt sample versus a change of 18 mV for the sample protected by a 3 nm $Nb_2O_5$ layer.

Electrochemical impedance spectroscopy (EIS) results have been summarized as Nyquist plots (Fig. 9a), capacitance plots (Fig. 9b), and normalized capacitance plots (Fig. 9c). In Fig. 9, the steepness of the slope for the bare Pt BOT compared to the niobia-coated sample indicates that the $Nb_2O_5$ film causes some increase of electronic resistance. While the bare Pt EOT plot displays less resistance than either of the coated samples, the increase in resistance after electrochemical cycling is greater for the bare Pt sample than for the $Nb_2O_5$-coated sample. These differences are better visualized as capacitance plots in Fig. 9b. The $Nb_2O_5$-coated sample has slightly lower capacitance than the bare Pt sample, but the change

in capacitance over time is clearly much greater for the bare Pt sample. By normalizing these plots to their maximum capacitance value (Fig. 9c), this difference is more easily noted.

The results described from Figs. 7 to 9 highlight that with prolonged electrochemical testing at the applied potentials, there is less degradation when the sample had a passivation film of $Nb_2O_5$ despite the materials insulating properties. The nanoscale coverage of the $Nb_2O_5$ layer did not induce a noteworthy reduction in platinum accessibility or a detrimental increase in electrical resistance during the electrochemical reaction, yet provides an enhanced chemical and electrochemical stability under degradation conditions that would be experienced in fuel cell environments. Future development and understanding of the interfaces created using ALD fabricated thin films can lead to intelligent design of passivation layers to protect nanofabricated fuel cell catalyst layers from degradation.

## Conclusion

In this paper, we have demonstrated the successful deposition of a nanometer-thin layer of $Nb_2O_5$ onto platinum using atomic layer deposition to act as a passivation layer to platinum dissolution during electrochemical cycling. A $Nb_2O_5$ layer with a thicknesses of 3 nm has been achieved, and the layer has been exposed to electrochemical cycling to evaluate resistance to platinum degradation conditions. The thickness of the layer was verified using SEM-FIB. To our knowledge, nanometer-thin $Nb_2O_5$ protective films produced to this nanometer scale have not been tested for their electrochemical stability to protect platinum for fuel cell applications. With improved understanding of the limits to these electronically conductive/electronically insulating interfaces, design and processing of fuel cell catalyst materials can be improved to meet future performance and durability targets.

## Acknowledgements

The authors acknowledge financial support from Mitacs (Elevate Grant No. IT05186) in collaboration with Automotive Fuel Cell Cooperation Corporation (J. Eastcott), the Mitacs Globalink Programs (A. Parakh), the Natural Sciences and Engineering Research Council (NSERC) of Canada (Discovery Grant No. 1077758), the Canada Research Chairs Program (B.D. Gates, Grant No. 950-215846), and MNT Financial Assistance (CMC Microsystems, Grant No. 4295). This work made use of the 4D LABS (www.4dlabs.ca) and the Centre for Soft Materials shared facilities supported by the Canada Foundation for Innovation (CFI), British Columbia Knowledge Development Fund (BCKDF), Western Economic Diversification Canada, and Simon Fraser University. The authors gratefully acknowledge the 4D LABS staff for their assistance and expertise related to this project.

## References

(1) US Office of energy efficiency & renewable energy. *Fuel Cell Technol. Off. Multi-Year Res. Dev. Demonstr. Plan* **2017**, 3.4.1.

(2) Holdcroft, S. *Chemistry of Materials*. 2014, pp 381–393.

(3) Mench, M. M.; Kumbur, E. C.; Veziroglu, T. N.; Kocha, S. S. In *Polymer Electrolyte Fuel Cell Degradation*; 2012; pp 89–214.

(4) Zhang, L.; Wang, L.; Holt, C. M. B.; Navessin, T.; Malek, K.; Eikerling, M. H.; Mitlin, D. *J. Phys. Chem. C* **2010**, *114* (39), 16463.

(5) Takenaka, S.; Mikami, D.; Tanabe, E.; Matsune, H.; Kishida, M. *Appl. Catal. A Gen.* **2015**, *492*, 60.

(6) Takabatake, Y.; Noda, Z.; Lyth, S. M.; Hayashi, A.; Sasaki, K. *Int. J. Hydrogen Energy* **2014**, *39,*

5074.

(7) Yan, L.; Rui, X.; Chen, G.; Xu, W.; Zou, G.; Luo, H. *Nanoscale* **2016**, *8*, 8843.

(8) Asselin, E.; Ahmed, T. M.; Alfantazi, A. *Corros. Sci.* **2007**, *49* (2), 694.

(9) Aegerter, M. A. *Sol. Energy Mater. Sol. Cells* **2001**, *68* (3–4), 401.

(10) Kim, H.-N.; Moon, J. H. *ACS Appl. Mater. Interfaces* **2012**, *4* (11), 5821.

(11) Blanquart, T.; Niinistö, J.; Heikkilä, M.; Sajavaara, T.; Kukli, K.; Puukilainen, E.; Xu, C.; Hunks, W.; Ritala, M.; Leskelä, M.; Leskela, M. *Chem. Mater.* **2012**, *24* (6), 975.

(12) Ma, X.; Chen, Y.; Li, H.; Cui, X.; Lin, Y. *Mater. Res. Bull.* **2015**, *66*, 51.

(13) Graça, M. P. F.; Saraiva, M.; Freire, F. N. A.; Valente, M. A.; Costa, L. C. *Thin Solid Films* **2015**, *585* (1), 95.

(14) Verma, A.; Singh, P. K. *Indian J. Chem. - Sect. A Inorganic, Phys. Theor. Anal. Chem.* **2013**, *52* (5), 593.

(15) Sreethawong, T.; Ngamsinlapasathian, S.; Yoshikawa, S. *Mater. Lett.* **2012**, *78*, 135.

(16) Amaravathy, P.; Sowndarya, S.; Sathyanarayanan, S.; Rajendran, N. *Surf. Coatings Technol.* **2014**, *244*, 131.

(17) Velten, D.; Eisenbarth, E.; Schanne, N.; Breme, J. *J. Mater. Sci. Mater. Med.* **2004**, *15* (4), 457.

(18) Orilall, M. C.; Matsumoto, F.; Zhou, Q.; Sai, H.; Abruña, H. D.; DiSalvo, F. J.; Wiesner, U. *J. Am. Chem. Soc.* **2009**, *131* (26), 9389.

(19) Rocha, T. A.; Ibanhi, F.; Colmati, F.; Linares, J. J.; Paganin, V. A.; Gonzalez, E. R. *J. Appl. Electrochem.* **2013**, *43* (8), 817.

(20) Sasaki, K.; Zhang, L.; Adzic, R. R. *Phys. Chem. Chem. Phys.* **2008**, *10* (1), 159.

(21) Varma, P. C. R.; Periyat, P.; Oubaha, M.; McDonagh, C.; Duffy, B. *Surf. Coatings Technol.* **2011**, *205* (16), 3992.

(22) Zhang, L.; Wang, L.; Holt, C. M. B.; Zahiri, B.; Li, Z.; Malek, K.; Navessin, T.; Eikerling, M. H.; Mitlin, D. *Energy Environ. Sci.* **2012**, *5* (3), 6156.

(23) Huang, S.-Y.; Ganesan, P.; Popov, B. N. *Appl. Catal. B Environ.* **2010**, *96* (1–2), 224.

(24) Chhina, H.; Campbell, S.; Kesler, O. *J. Electrochem. Soc.* **2009**, *156* (10), B1232.

(25) Graca, M. P. F.; Meireles, a; Nico, C.; Valente, M. a. *J. Alloys Compd.* **2013**, *553*, 177.

(26) Sreethawong, T.; Ngamsinlapasathian, S.; Lim, S. H.; Yoshikawa, S. *Chem. Eng. J.* **2013**, *215–216*, 322.

(27) Sabarirajan, D. C.; Vlahakis, J.; White, R. D.; Zenyuk, I. V. *ECS Trans.* **2016**, *75* (14), 747.

(28) Huang, Y.; Xu, Y.; Ding, S.-J.; Lu, H.-L.; Sun, Q.-Q.; Zhang, D. W.; Chen, Z. *Appl. Surf. Sci.* **2011**, *257* (16), 7305.

(29) Pizzutilo, E.; Geiger, S.; Grote, J.-P.; Mingers, A.; Mayrhofer, K. J. J.; Arenz, M.; Cherevko, S. *J. Electrochem. Soc.* **2016**, *163* (14), 1510.

(30) Easton, E. B.; Pickup, P. G. *Electrochim. Acta* **2005**, *50* (12), 2469.

**Table 1.** Electrochemically active surface area (ECSA) before (BOT: beginning of test) and after (EOT: end of test) 5 000 sequential scans of the applied potential for a bare platinum film and for platinum films covered with 3-nm thick $Nb_2O_5$ film.

| sample | geometric surface area ($cm^2$) | BOT ECSA ($m^2/g$) | EOT ECSA ($m^2/g$) | decrease in ECSA with cycling (%) |
|---|---|---|---|---|
| bare Pt | 1.8 | 0.719 ± 0.054 | 0.475 ± 0.004 | 33.7 ± 5.0 |
| Pt + 3 nm $Nb_2O_5$ | 2 | 0.669 ± 0.006 | 0.492 ± 0.008 | 26.5 ± 1.7 |

## Figure Captions

**Fig. 1.** The atomic layer deposition (ALD) process for thin film deposition: a silicon wafer with a thin Pt film (ca. 200 nm) was used as the substrate. Precursors were sequentially introduced into the ALD chamber to grow a thin film of $Nb_2O_5$ (~3 nm).

**Fig. 2.** Half-cell electrochemical set-up used to evaluate the nanoscale coating of $Nb_2O_5$ on platinum surfaces.

372 **Fig. 3.** Profilometry of the thin metal film consisting of a ca. 200-nm thick platinum layer deposited on an
373 ~5-nm thick chromium adhesion layer supported on a polished silicon wafer.

374

375 **Fig. 4.** A representative energy dispersive X-ray spectroscopy (EDS) based spectrum for the 3-nm thick
376 niobium oxide film on a Pt layer.

377

378 **Fig. 5.** Individual EDS maps obtained in conjunction with high resolution TEM analyses of (a) platinum,
379 (b) niobium, (c) oxygen, and (d) iridium for a cross section of the ~3-nm thick films of supported $Nb_2O_5$.
380 The scale bar in each image has a length of 10 nm.

381

382 **Fig. 6.** Overlapping high resolution EDS maps at (a) 450 000x magnification and (b) 900 000x
383 magnification of the ~3-nm thick $Nb_2O_5$ coating on a platinum substrate, which was prepared by a FIB
384 lift-out process. Black region = carbon layer. The scale bars for (a) and (b) are 20 and 10 nm,
385 respectively.

386

387 **Fig. 7.** The initial cyclic voltammetry (CV) scans of the bare Pt prepared by physical vapour deposition or
388 PVD (black solid line) and the Pt PVD (red dashed line) coated with a 3-nm thick $Nb_2O_5$ layer. These
389 studies were performed at a scan rate of 50 mV $s^{-1}$.

390

391 **Fig 8.** Linear sweep voltammetry (LSV) for bare Pt PVD samples (black lines) and the Pt PVD coated with
392 a 3-nm thick $Nb_2O_5$ layer (red lines) at BOT (solid line) and EOT (dotted line). These studies were
393 performed at a scan rate of 5 mV $s^{-1}$.

394

395 **Fig 9.** Electrochemical impedance spectroscopy (EIS) plots for bare Pt PVD samples (black lines; solid

396 symbols) and the 3-nm $Nb_2O_5$ layer (red lines; open symbols) at BOT (solid line) and EOT (dotted line).

397 Plots include (a) Nyquist plot, (b) capacitance plot, and (c) normalized capacitance plot.

398

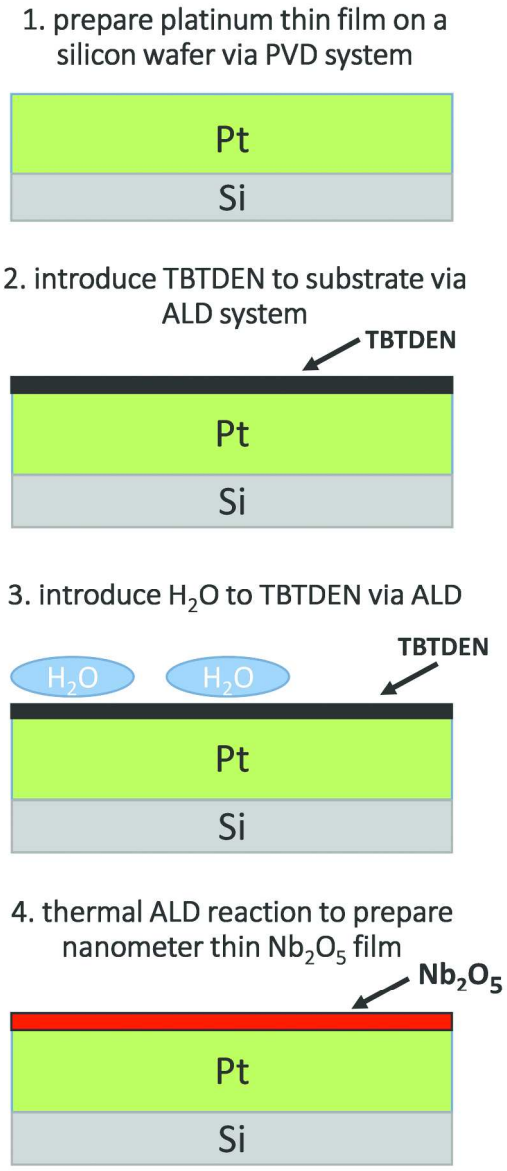


Figure 1

190x438mm (300 x 300 DPI)

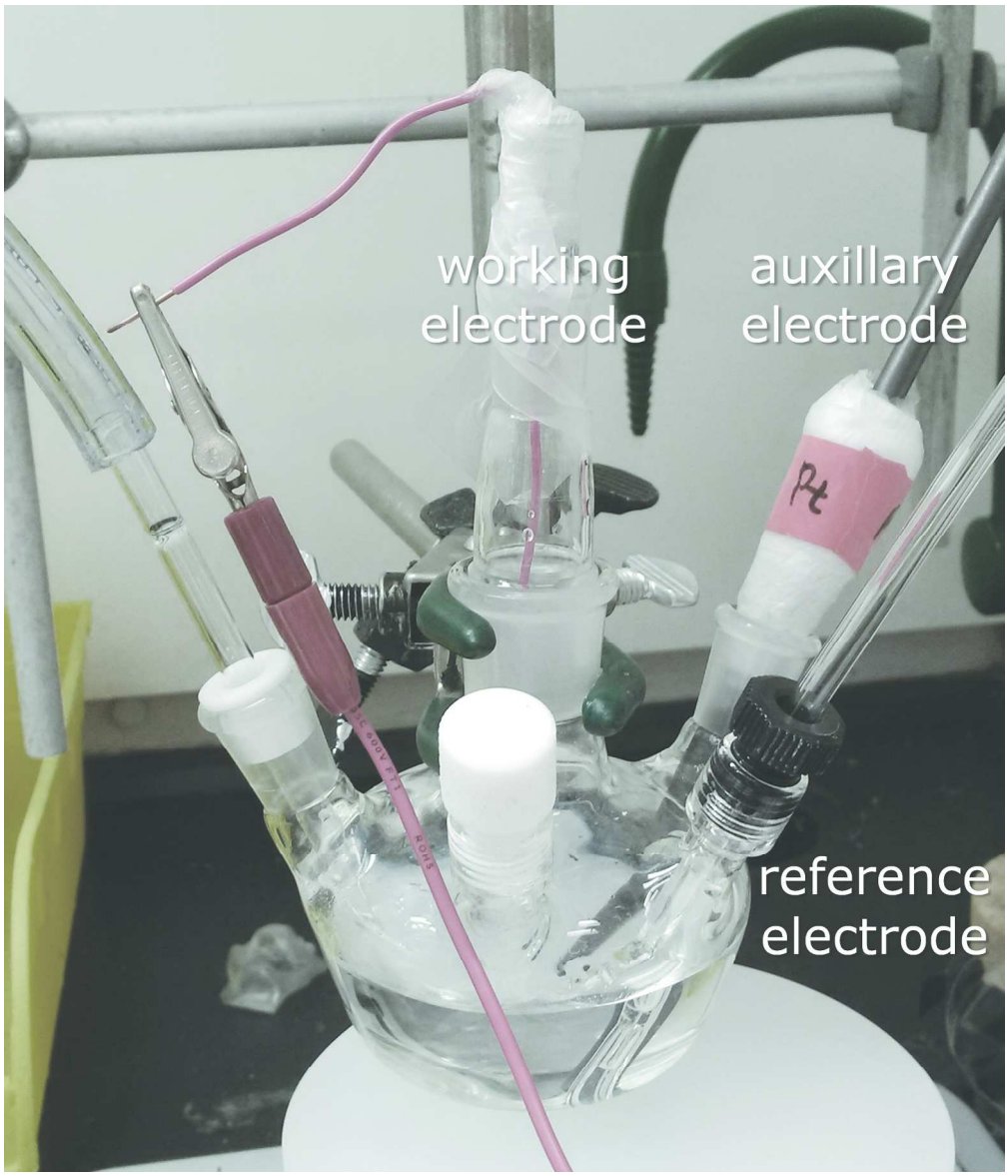


Figure 2

96x112mm (600 x 600 DPI)

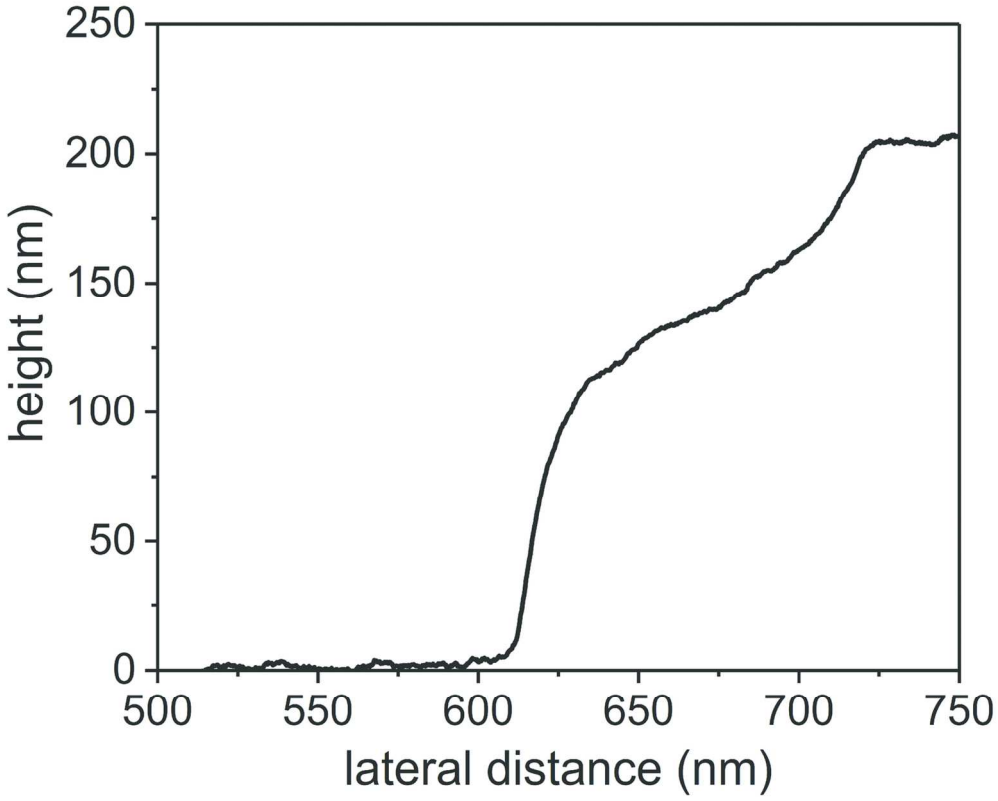


Figure 3

65x52mm (600 x 600 DPI)

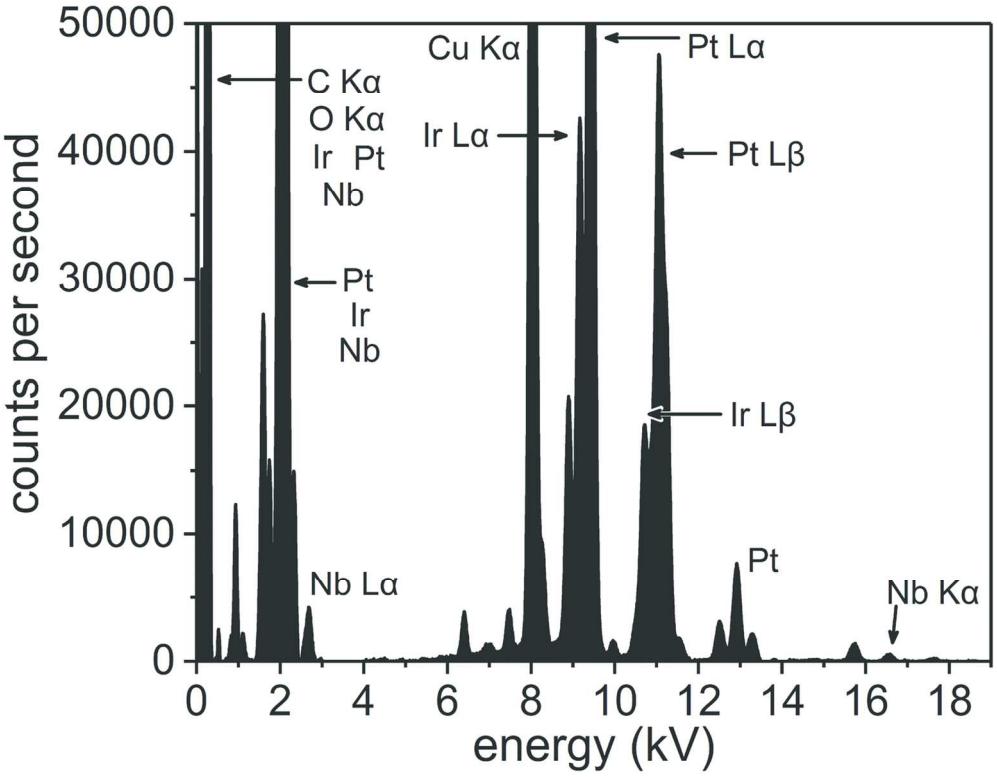


Figure 4

64x49mm (600 x 600 DPI)

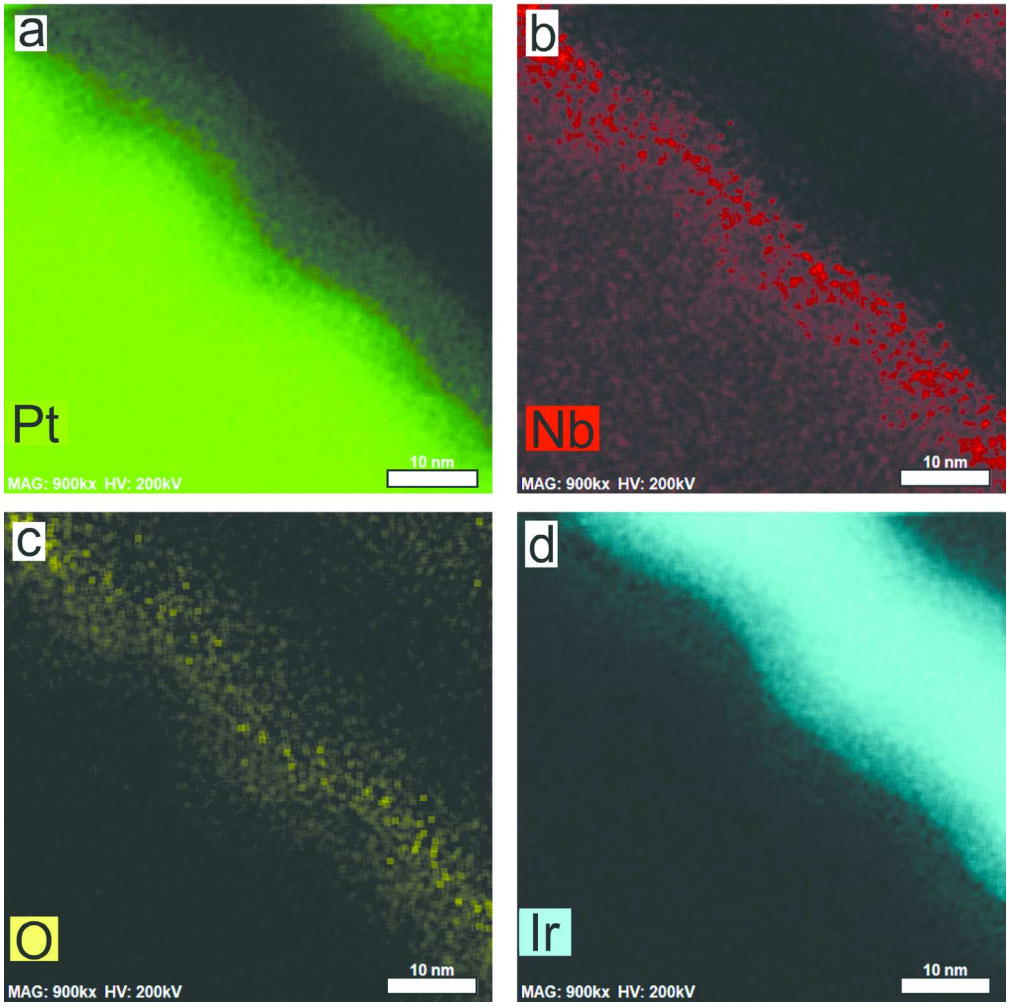


Figure 5

166x166mm (300 x 300 DPI)

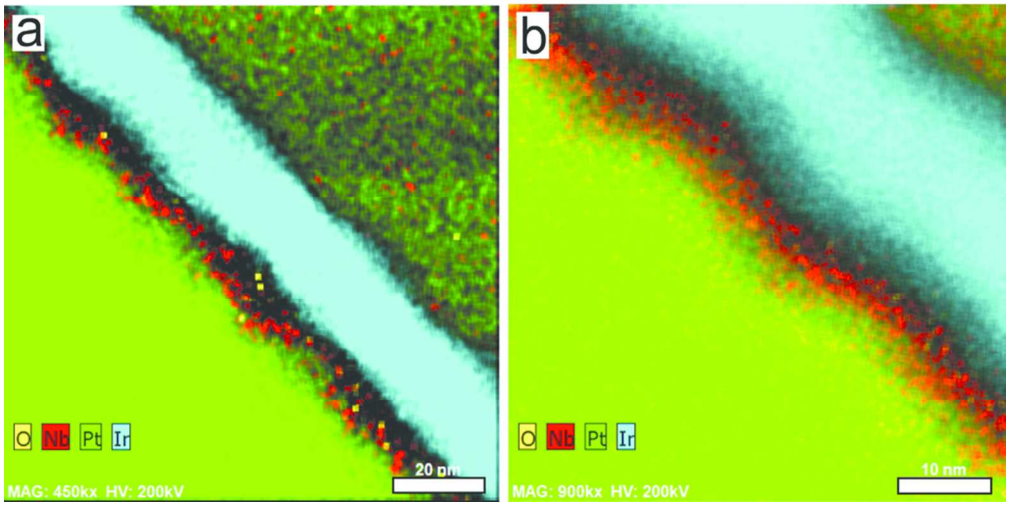


Figure 6

83x42mm (300 x 300 DPI)

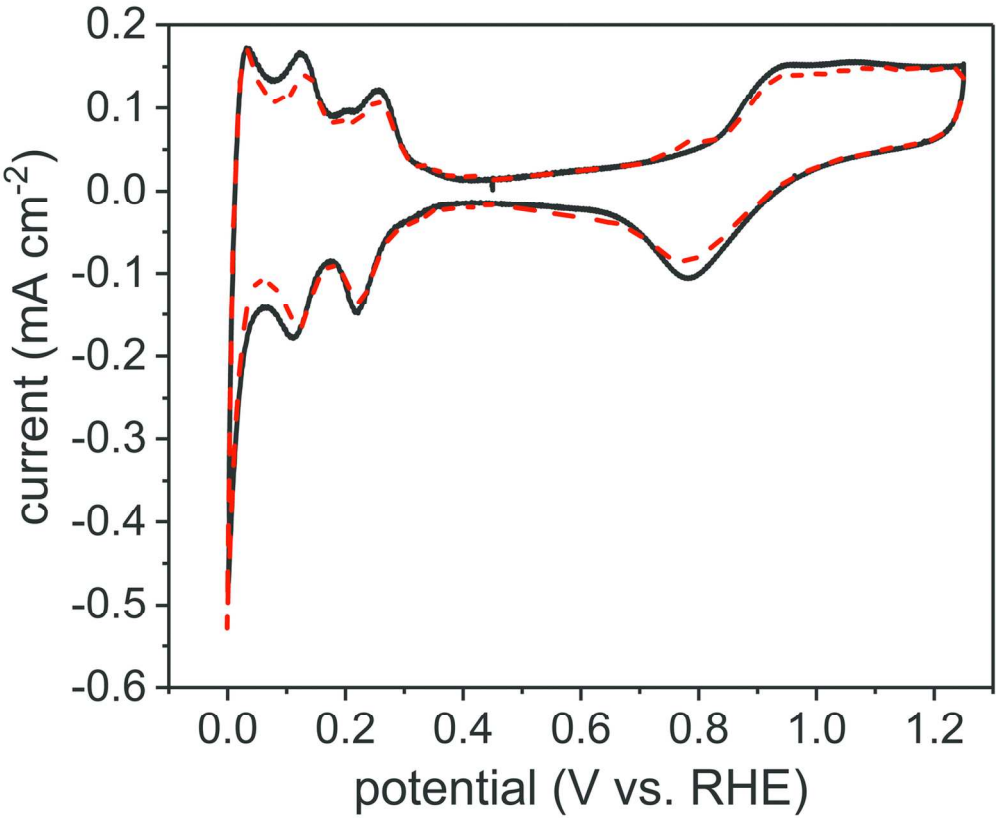


Figure 7

67x55mm (600 x 600 DPI)

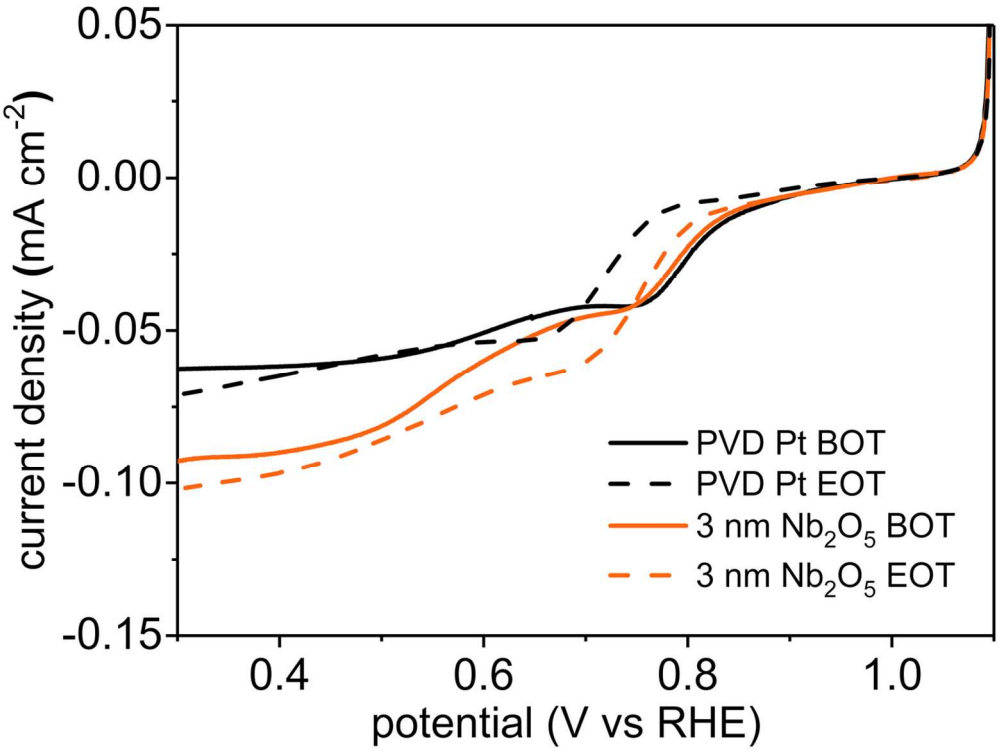


Figure 8

62x46mm (600 x 600 DPI)

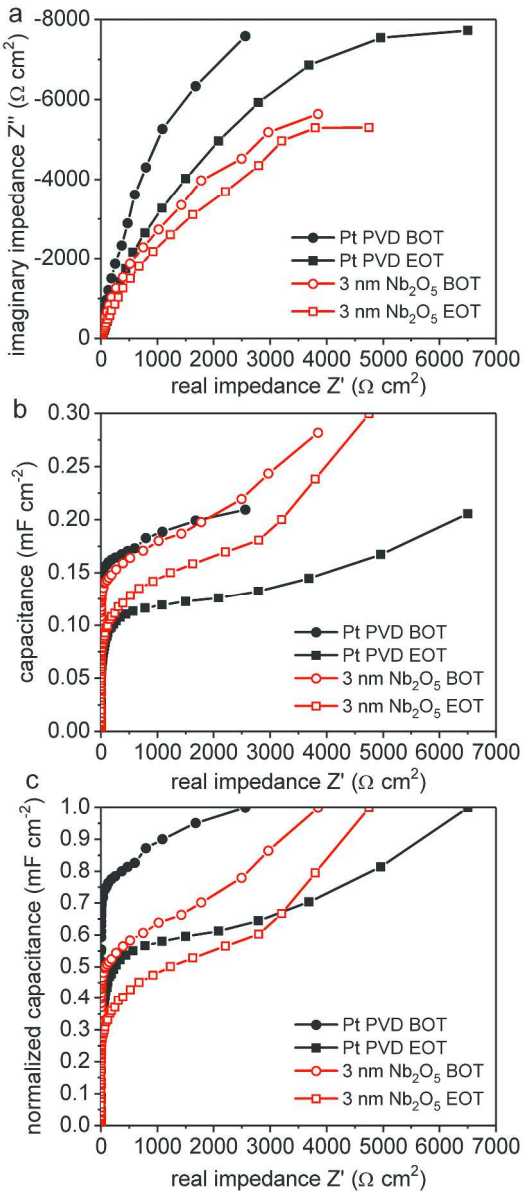


Figure 9

187x424mm (600 x 600 DPI)